frontiers | Frontiers in Energy Research

TYPE Methods
PUBLISHED 26 January 2023
DOI 10.3389/fenrg.2022.1055405

OPEN ACCESS

EDITED BY
Jingang Liang,
Tsinghua University, China

REVIEWED BY
Jinsen Xie,
University of South China, China
Chenglong Wang,
Xi'an Jiaotong University, China

*CORRESPONDENCE
Lianjie Wang,
wanglianjie@npic.ac.cn

SPECIALTY SECTION
This article was submitted to Nuclear Energy,
a section of the journal
Frontiers in Energy Research

RECEIVED 27 September 2022
ACCEPTED 28 November 2022
PUBLISHED 26 January 2023

CITATION
Zhang B, Wang L, Lou L, Zhao C, Peng X, Yan M, Xia B, Zhang C, Qiao L and Wu Q (2023), Development and verification of lead-bismuth cooled fast reactor calculation code system Mosasaur. *Front. Energy Res.* 10:1055405. doi: 10.3389/fenrg.2022.1055405

Development and verification of lead-bismuth cooled fast reactor calculation code system Mosasaur

Bin Zhang, Lianjie Wang*, Lei Lou, Chen Zhao, Xingjie Peng, Mingyu Yan, Bangyang Xia, Ce Zhang, Liang Qiao and Qu Wu

Science and Technology on Reactor System Design Technology Laboratory, Nuclear Power Institute of China, Chengdu, Sichuan, China

Lead-bismuth cooled fast reactor calculation code system named MOSASAUR has been developed to meet the simulation requirements from LBFR engineering design. An overview of MOSASAUR developments is provided in this paper, four main functional modules and their models are introduced: cross-sections generation module, flux spectrum correction module, core simulation module and sensitivity and uncertainty analysis module. Verification and validation results of numerical benchmark calculations, code-to-code comparisons with the Monte-Carlo code and critical experimental calculations shown in this paper prove the capabilities of MOSASAUR in dealing with lead-bismuth cooled fast reactor analysis problems with good performances. Numerical results demonstrate that compared with the Monte-Carlo code, the relative errors of eigenvalues are smaller than 350pcm when the calculations were carried out with the same nuclear data file. Compared with the measured values, the errors will increase due to the simulation details and the measurement accuracy.

KEYWORDS

lead-bismuth cooled fast reactor, cross-sections generation, flux spectrum correction, core simulation, sensitivity and uncertainty, verification and validation

1 Introduction

Due to the hard neutron spectrum, fast reactors have significant advantages in utilization rate of the nuclear energy resources and incineration of long-lived nuclear waste (Bouchard and Bennett, 2008). The fast reactors play an important role among the six candidate types of the fourth generation of nuclear power. Lead-based cooled advanced reactor, a fourth-generation nuclear reactor system, uses liquid metal as coolant. The excellent performances of lead-bismuth which is used as the reactor coolant in Lead-bismuth cooled fast reactor (LBFR) bring the reactor significant advantages in physical characteristics and safe operation. Firstly, the LBFR has high utilization rate of resources. Lead-based materials have lower neutron slowing capacity and smaller capture cross-sections. The reactor core is designed with a harder neutron

energy spectrum, which can take advantages of neutrons for nuclear fuel regeneration and nuclear waste transmutation (Hu and Yuan, 1995). The reactor can achieve long core life and is helpful to prevent nuclear proliferation. Secondly, the LBFR has good thermal safety and security (Xu, 2009). The lead-based materials have high thermal conductivity, low melting point, high boiling point and other characteristics. It makes that the reactor can be operated at atmospheric pressure and can achieve high power density. The higher thermal expansion rate of lead-based materials and lower kinematic viscosity coefficient can ensure that the reactor has sufficient natural cycling capacity. What's more, the chemical safety is good. The lead-based materials are chemically inactive and hardly react with water and air, which make the violent chemical reaction impossible. Thirdly, the LBFR has good economy. Lead-bismuth cooled fast reactor eliminates the need for large high-pressure vessels, have simple auxiliary systems, and have low construction and operation and maintenance costs.

The research and development of fast reactors has been pushed globally in recent decade, including in China. The China lead-based reactor (Wu, 2016) and the lead-bismuth eutectic (LBE)–cooled China initiative accelerator driven subcritical system (Liu et al., 2017) have been proposed by two institutes of the Chinese Academy of Sciences.

One of the most important elements of the fast reactor core design is the core neutronics computational analysis. At present, there are two main kinds of calculation methods. First is the one-step calculation method (Rachamin and Kliem, 2017), which is used to simulate the core directly with as few approximations as possible. The other one is the two-step calculation method which is based on the homogenization techniques (Zhang et al., 2016). For the whole core physics simulation, the computational cost of one-step calculation with fully detailed description is too expensive using either stochastic (Wang et al., 2015) or deterministic method (Downar et al., 2016) even with the currently most advanced computing powers. So even though one-step calculation method has a lot of advantages, the dominant method for fast core simulation is the two-step scheme.

In the two-step scheme, the Monte Carlo codes is becoming popular to generate few-group cross-sections for the whole core calculation with the improvement of computer technique and the development of Monte Carlo method in recent decades. The Serpent code has been proven to be feasible (Nikitin et al., 2015), and similar work has also been researched in MCNP (Heo et al., 2013) and TRIPOLI (Cai, 2014). Due to sufficient computational accuracy and high computational efficiency, deterministic procedures are currently the most widely used simulation methods.

In China, the fast reactor code system SARAX (Zheng et al., 2018a; Zheng et al., 2018b) developed by Xian Jiaotong University is well known. The TULIP code is used to generate the 33-group cross-sections, which is based on the 1968-group cross-sections libraries from NJOY (Macfarlane and MUIR, 1994). The narrow resonance approximation (Lee and Yang, 2012) is applied for the resonance calculation. Alternatively, the embedded one-dimensional Monte Carlo calculation is applied as an option to get the ultrafine-group cross-sections. The LEVENDER code is used for the core simulation which is based on the S_N transport equations.

The MC^2/The DIF3D/REBUS system is the best-known fast reactor code system in the United States. MC^2 (Henryson et al., 1973) uses the library generated from ETOE-2 and solves the ultrafine-group (2082 groups) slowing-down equations for different compositions and temperatures to generate the few-group cross-sections. The DIF3D (Derstine, 1984) and code VARIANT (Palmiotti et al., 1995) are used to solve the neutron equations which is applied in REBUS to do the fuel cycle analysis. The ERANOS system is the most widespread in Europe which generates the cross-sections by ECCO (Grimstone, 1990). The subgroup method based on the probability tables is applied for the resonance calculation. The CONSYST-TRIGEX code system is used for fast reactor core simulation in Russia.

In order to improve the accuracy of legacy fast reactor codes, new methods and models have been researched. The two-dimensional capability and calculation of hyper fine group (~400,000 groups) slowing-down equation (Lee and Yang, 2012) were extended in MC^2/DIF3D. A new self-shielding method (Li Z et al., 2017) and new homogenization techniques have been implemented in APOLLO-3 code (Archier et al., 2016). The neutron transport solver is becoming popular in the fast reactor core calculation (Shemon et al., 2017).

In this paper, an overview of the **MO**delling and **S**imul**A**tion code system for neutronic**S** of le**A**d bism**U**th cooled **R**eactor named MOSASAUR is provided which is developed to meet the LBFR engineering design requirements by Nuclear Power Institute of China (NPIC), China National Nuclear Corporation (CNNC). Main functional modules and their models contained in MOSASAUR are introduced in Section 2. Section 3 gives the numerical results of the verification and validation. Section 4 summarizes this paper.

2 Modules of mosasaur

The deterministic two-step calculation strategy based on the homogenization theory is utilized in MOSASAUR to perform the reactor core neutronics analysis. In the first step, the cross-sections generation module named MOCS is used the narrow resonance approximation to solve the resonance problem. For the typical assemblies, ultrafine-group cross-sections and neutron flux will be determined and the few-group homogenized cross-sections will be collapsed based on the flux-volume weight method and the principle of conservation of reaction rate. The calculation process of MOCS is shown in Figure 1.

The homogenized few-group cross-sections are based on the single assembly calculation which is under the reflective boundary

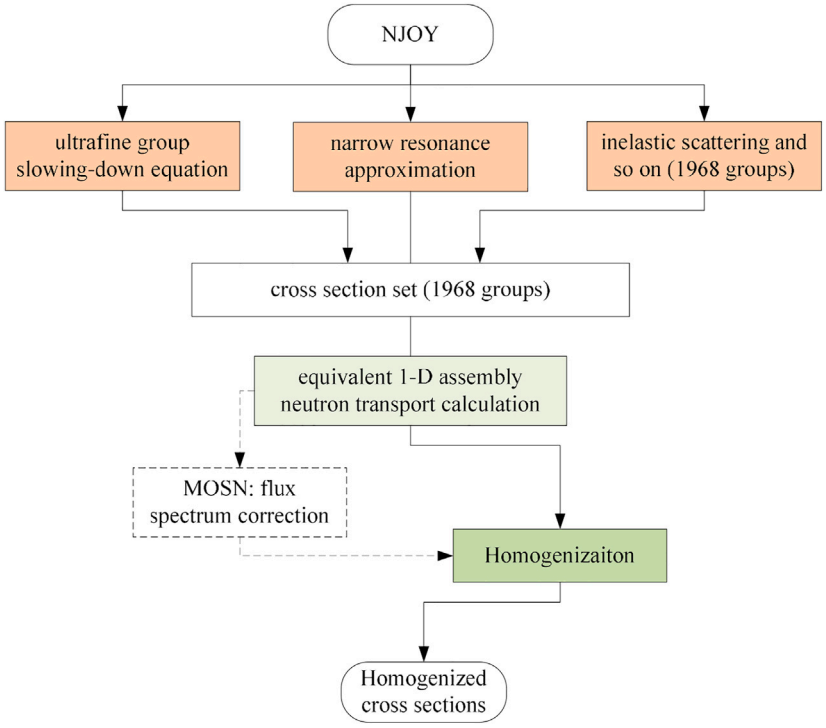

FIGURE 1
The calculation process of MOCS.

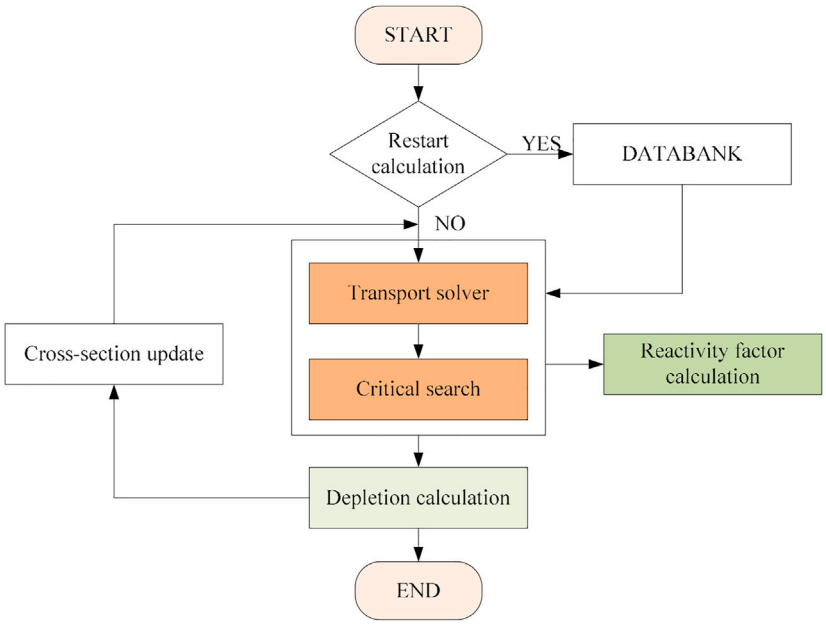

FIGURE 2
The calculation process of MOCO.

condition. It is different from the actual environment of the assembly in the actual core position. Therefore, the second step is optional to perform an equivalent two-dimensional whole core calculation by the flux spectrum correction module named MOSN to modify the single-assembly neutron energy spectrum.

Core simulation module MOCO is used to simulate core neutron behaviors based on the neutron transport solvers and depletion calculation and so on. The calculation process is shown in Figure 2. Besides the neutron flux and burnup calculation, critical research base on the control rod and reactivity coefficients calculation have been developed in MOCO.

For a complete LBFR simulation, both of MOCS and MOCO are indispensable. MOCS is used to generate the homogenized few-group cross sections in advanced for all types of assemblies. Based on the few-group constants, MOCO will be used to simulate the whole reactor core. Due to the whole-core spatial coupling effect, MOSN is applied to modify the flux of MOCS. In the process of the simulation, the data between the three modules is transferred through files.

Finally, the sensitivity and uncertainty analysis module called SUN will be used to evaluate and quantify the confidence of the calculated results. The SUN module will call MOCS as a black box to generate the perturbed multi-group cross-sections, and call MOCO as a black box to get the results of response quantities.

2.1 MOCS: Cross-sections generation module

In order to balance computational accuracy and efficiency, an equivalent one-dimensional assembly is modeled in MOCS. The coupling method based on the narrow resonance approximation and the ultrafine group method is utilized to deal with the complex resonance effect in LBFR. Due to the plausibility in the high energy range, the resonance calculation method based on the narrow resonance approximation is used. As the energy decreases, the error introduced by the narrow resonance approximation gradually increases. So below the energy divider, ultrafine group slowing-down equations are solved to accurately simulate the neutron slowing process directly, which can avoid the error brought by the narrow resonance approximation.

In the high energy range, the effective resonant self-screening cross-sections based on the narrow resonance approximation is calculated as follows:

$$\bar{\sigma}_{x,i,g} = \frac{\int_{\Delta E_g} \sigma_{x,i}(E)\phi(E)dE}{\int_{\Delta E_g} \phi(E)dE} \approx \int_{\Delta E_g} \sigma_{x,i}(E)\frac{\sum_p(E)}{E.\sum_t(E)}dE \Big/ \int_{\Delta E_g} \frac{\sum_p(E)}{E.\sum_t(E)}dE \quad (1)$$

where $\sigma_{x,i}(E)$ is the point-wise cross-section of type x for the resonant isotope i at the energy point E, and ΔE_g is lethargy width in the energy group g.

The potential scattering cross-sections is assumed to be constant in each energy group, so the equation can be further simplified as follows:

$$\bar{\sigma}_{x,i,g} \approx \int_{\Delta E_g} \frac{\sigma_{x,i}(E)}{E \cdot \Sigma_t(E)}dE \Big/ \int_{\Delta E_g} \frac{1}{E \cdot \Sigma_t(E)}dE \quad (2)$$

The elastic scattering matrix is divided into two parts: the total effective elastic scattering cross-sections and the scattering function. Since the information of elastic scattering cross-sections and total cross-sections are given in the form of point cross-sections in the database, the total effective elastic scattering cross-sections can be solved by Eq. 2. The scattering function is calculated as follows:

$$\sigma_s^l(g \to g') = \bar{\sigma}_{s,g}.F(l,\alpha, g \to g') \quad (3)$$

$$F(l,\alpha, g \to g') = \frac{\int_{\Delta E_g}\int_{\Delta E_{g'}} \frac{p_l(\mu_s(E,E'))}{E} \sum_{n=0}^{N}(2n+1)a_n(E)p_n(\mu_c(E,E'))dEdE'}{\Delta E_g(1-\alpha)} \quad (4)$$

Like the elastic scattering matrix, the scattering matrix of the inelastic scattering reaction and the threshold energy reaction also represents the probability of the corresponding reaction. Compared with the elastic scattering reaction, the cross-sections of the inelastic scattering reaction and the threshold energy reaction is flatter with energy, and its resonance effect is much weaker than that of the elastic scattering reaction. Therefore, the scattering matrix of such reactions is less relevant to the problem and is produced in advance in MOCS.

The collision probability method (CPM) is used to determine the neutron flux based on the cross-sections as follows:

$$\phi_{0,g,r} = \sum_{r'}\left[\sum_{g'}\left(\Sigma_{s,0,g'\to g,r'} + \frac{\chi_g}{k_{eff}}\upsilon\Sigma_{f,j,g'}\right)\phi_{0,g',r'}\right]\frac{P_{r\to r',g}V_{r'}}{\Sigma_{t,g,r}V_r} \quad (5)$$

Below the energy divider, the ultrafine group method solves the neutron slowing process precisely to eliminate the approximate. In the lower energy range, MOCS neglects the inelastic scattering source term as well as the fission source term, and set cross-sections as a constant in each ultrafine group. The slowing down equations are as follows:

$$\sum_{r,h}^{t}\phi_{r,h}V_r = \sum_{r'} p_{r'\to r,h}V_{r'}\sum_i s_{i,h} \quad (6)$$

$$s_{i,h} = \sum_{h'=1}^{H} N_{r^i,i}\sigma^e_{r',i,h-h'}\phi_{r',h-h'}p_{i,h'} \quad (7)$$

Without using the flux spectrum correction module MOSN, the neutron flux for the equivalent one-dimensional assembly would be calculated in MOCS to collapse the cross-sections from 1968 groups into 33 groups. In the homogenization process, the super homogenization method (SPH method) (Hebert, 2009) is optional to be used as the homogenization technique. In order to

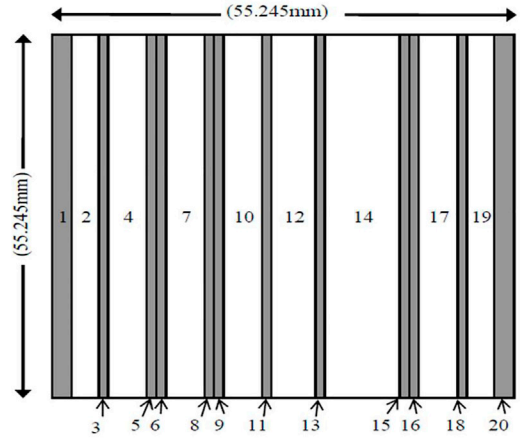

1	:	Matrix & Drawer side wall (2.2225mm)
2	:	Thin Fe_2O_3 plate (3.175mm)
3	:	Can wall (0.381mm)
4	:	ZPPR-Pu fuel (5.588mm)
5	:	Can wall (0.381mm)
6	:	Can wall (0.381mm)
7	:	Sodium (5.588mm)
8	:	Can wall (0.381mm)
9	:	Can wall (0.381mm)
10	:	Na_2CO_3 (5.588mm)
11	:	Can wall (0.381mm)
12	:	U_3O_8 plate (6.35mm)
13	:	Can wall (0.381mm)
14	:	Sodium (11.938mm)
15	:	Can wall (0.381mm)
16	:	Can wall (0.381mm)
17	:	ZPPR-Pu fuel (5.588mm)
18	:	Can wall (0.381mm)
19	:	Thin Fe_2O_3 plate (3.175mm)
20	:	Matrix & Drawer side wall (2.2225mm)

FIGURE 3
Geometry and layout of the ZPPR-10B assembly.

get the cross-sections of the non-fuel assemblies, the multi-zone homogenization calculations would be carried out to determine the SPH factor in MOCS. The cross-sections are modified as follows:

$$\tilde{\Sigma}^{hom}_{x,i,g} = \mu_{i,g}\Sigma^{hom}_{x,i,g} \tag{8}$$

2.2 MOSN: Flux spectrum correction module

Due to the obvious whole-core spatial coupling effect and strong energy spectrum interference effect in the LBFR, A two-dimensional equivalent core is modeled to represent the actual reactor core for the flux spectrum correction in MOSN. The two-dimensional cylindrical core is simplified by using the volume equivalence method.

The two-dimensional core transport calculation is carried out based on the 1968-group cross-sections. The neutron flux of each assembly will be modified to collapses the 33-group cross-sections for use in the MOCO. The S_N method with parallel capability is applied to solve the transport equations in MOSN.

2.3 MOCO: Core simulation module

Based on the 33-group cross-sections generated by MOCS and MOSN, the core simulation is carried out by MOCO. The S_N method with triangular grid is applied as the solver of the transport equations. Functions such as depletion, critical search and reactivity coefficient calculation are included in MOCO.

The three-dimensional multi-group neutron transport equation within the triangular prism grid can be written as follows. MOCO assumes that the fission source is isotropic and scattering sources is anisotropic in the derivation.

$$\mu^m \frac{\partial \Psi^m_g(x,y,z)}{\partial x} + \eta^m \frac{\partial \Psi^m_g(x,y,z)}{\partial y} + \frac{\xi^m}{h_z}\frac{\partial \Psi^m_g(x,y,z)}{\partial z} + \Sigma^g_t \Psi^m_g(x,y,z) = \hat{Q}_g(x,y,z) \tag{9}$$

where m represents a certain angular direction, μ^m, η^m, ξ^m is the component of the angular direction m on the coordinate axis (x, y, z), $\Psi^m_g(x,y,z)$ is the angular flux of the g-th group.

In LBFR, besides of the heat generated by the fission reaction, the energy produced by the capture reaction of neutrons and by the reaction of photons is an important part of the whole power. In order to estimate the energy accurately without much cost, it was assumed that the energy of neutrons produces only from fission reaction and capture reaction, and the energy of photons is deposited at the place where the corresponding reaction occurs. The core power is calculated as the following equation:

$$P = \sum_g \sum_i N_i \left\{ k_i \sigma_{f,i,g} + q_{c,i}\sigma_{c,i,g} - q_{loss} \right\} \phi_g \tag{10}$$

where k_i and $q_{c,i}$ represent the energy produced by each fission reaction and by each radiation capture reaction of nuclide i. $\sigma_{f,i,g}$ and $\sigma_{c,i,g}$ is the fission cross-section and capture cross-section of g-th group, and q_{loss} is the energy lost:

$$q_{loss} = \left[(\nu - 1)\sigma_{f,i,g} - \sigma_{c,i,g} \right] \bar{E} \tag{11}$$

TABLE 1 The k_{inf} results of different assemblies.

Assemblies	k_{inf} of OpenMC	k_{inf} of MOCS	Raltive error/pcm
ZPPR-10B	1.13258	1.13383	125
MET-1000	1.30775	1.30944	169
JOYO	0.18316	0.18142	−174

TABLE 2 Geometric and material parameters of the critical experiments.

Parameters	HMF27	PMF35	HMF57-1	HMF57-2
Fuel	^{235}U	^{239}Pu	^{235}U	^{235}U
Enrichment (%)	90	98	93.17	93.17
Reflector	lead	lead	lead	lead
Radius of center cavity (cm)	1.019	1.2	0.555	0.555
Thickness of fuel (cm)	7.331	4.8	6.555	6.9235
Thickness of reflector (cm)	3.25	3.15	17.22	8.99
Temperature (K)	293	293	293	293

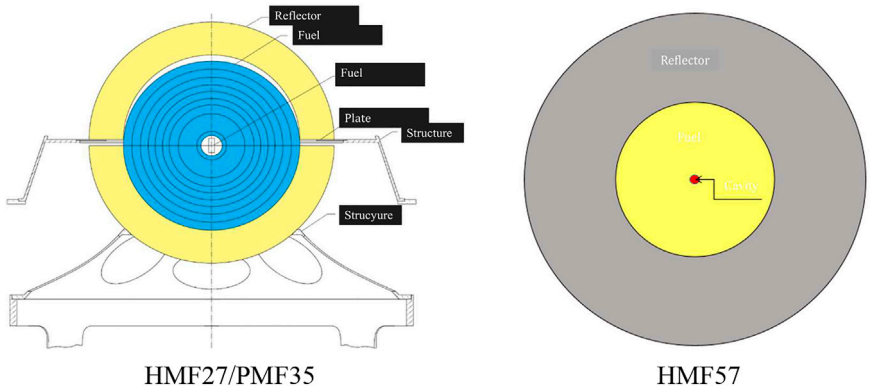

FIGURE 4
Diagrams of lead-based critical experiments.

$$\bar{E} = \frac{\sum \bar{E}_g \phi_g}{\sum \phi_g}, \quad \bar{E}_g = \frac{E_{g=1} - E_g}{\log\left(E_{g+1} / E_g\right)} \tag{12}$$

The micro-depletion scheme is applied to simulate the core burn up and the Chebyshev Rational Approximation Method (CRAM) is used to solve the depletion equation. In MOCO, three different depletion chains, 11 heavy isotopes, 21 heavy isotopes and 118 heavy isotopes, are provided as different options for different core system. For the LBFR, the chain which contains 21 heavy isotopes and 49 fission products is usually used for core simulation.

Considering the weak feedback effect of LBFR, the combination of the direct method and the perturbation theory is used to determine the reactivity coefficients. Based on the neutron transport equation, the form of the perturbation equation can be written as follow:

$$\langle \phi^* \left| \delta (L - \lambda F) \phi \right\rangle = 0 \tag{13}$$

where ϕ^* is the adjoint flux.

TABLE 3 The k_{inf} results of lead-based critical experiments.

Code	Nuclear data file	HMF27 k_{inf}	PMF35 k_{inf}	HMF57-1 k_{inf}	HMF57-2 k_{inf}
		±variance	±variance	±variance	±variance
Measured value	-	1.00000	1.00000	1.00000	1.00000
		±0.00250	±0.00160	±0.00200	±0.00230
MOCS	ENDF/B-VII.0	0.99993	0.99674	0.98870	0.99727
MCNP	ENDF/B-VII β3	1.00070	0.99790	0.98970	0.99850
		±0.00010	±0.00010	±0.00010	±0.00010
MCNP	ENDF/B-VI.8	1.00590	1.00800	1.00230	1.0087
		±0.00010	±0.00010	±0.00010	0 ± 0.00010
KENO	299group ABBN-93	0.99910	0.99830	0.98990	0.99820
		±0.00030	±0.00090	±0.00010	±0.00010

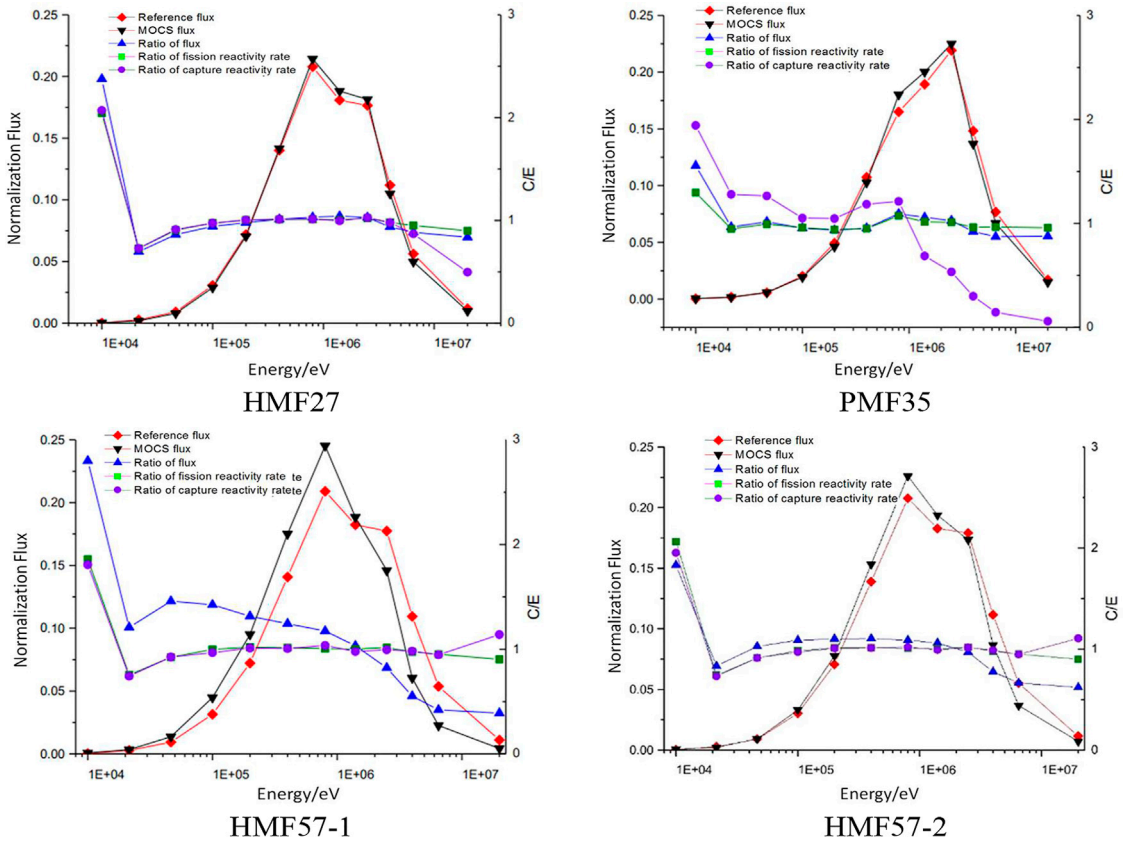

FIGURE 5
Flux and reactivity rate Results of HMF27 and PMF35.

TABLE 4 Results of fission reactivity rate and capture reactivity rate.

Reaction	Nuclide	HMF27		Nuclide	PMF35	
		reference	MOCS		reference	MOCS
Ratio of fission reactivity rate (%)	^{234}U	0.8	0.8	^{239}Pu	94.5	95.4
	^{235}U	86.7	86.8	^{240}Pu	1.1	1.2
	^{238}U	1.4	1.4	^{239}Pu	4	3.3
Ratio of capture reactivity rate (%)	^{234}U	0.2	0.1	^{240}Pu	0.1	0.1
	^{235}U	10.2	10.2	Ga	0.1	0.1
	^{238}U	0.7	0.7	Ni	0.2	0.0

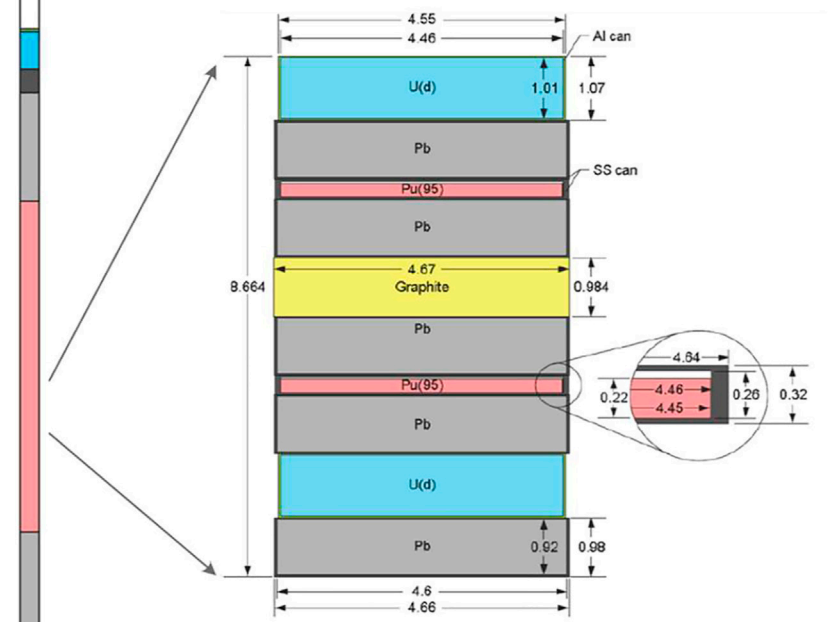

FIGURE 6
Layout of the fuel unit.

2.4 SUN: Sensitivity and uncertainty analysis module

The SUN module is mainly used to perform a sensitivity analysis and quantify uncertainty for the core simulation.

The Latin hypercube sampling method is used to generate the library of the perturbed multi-group cross-sections. The consistency of the perturbed cross-sections is maintained in the process of the cross-section perturbation and MOCO is used to perform the core simulation based on all samples of

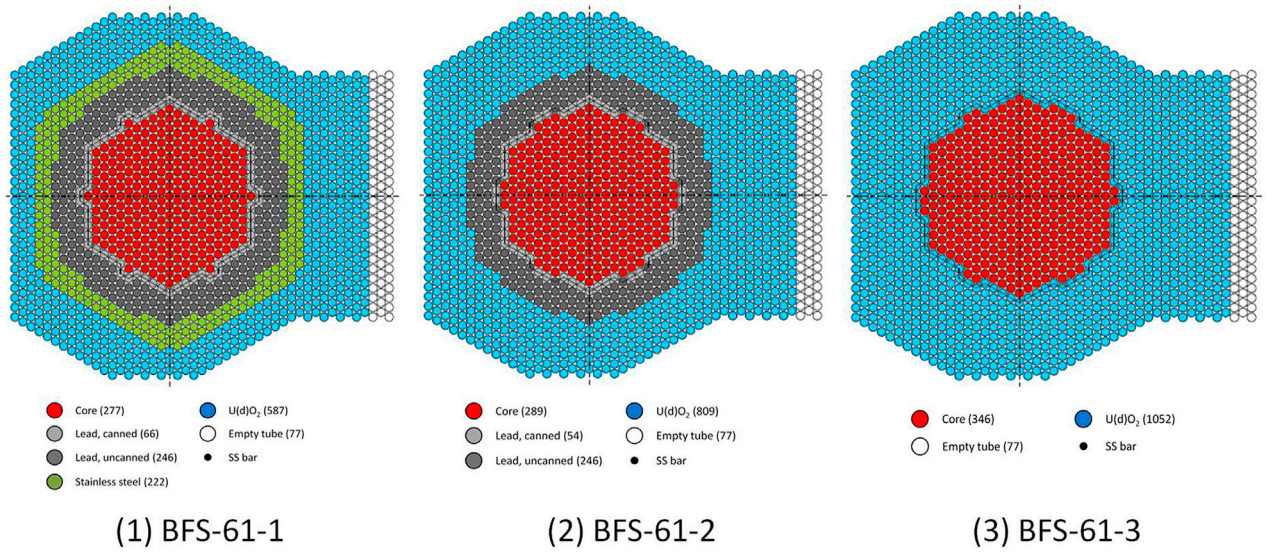

FIGURE 7
Core layout of BFS-61.

TABLE 5 Summary of the eigenvalue results of BFS-61.

CORE	Measured value ±variance	MCNP k_{inf} ±variance	MOOC k_{inf}	Difference with measured value/pcm	Difference with MCNP/pcm
BFS-61-1	1.00030	1.0006	0.99487	−545.6	−305.2
	±0.0029	±0.0002			
BFS-61-2	1.00040	0.9978	0.99349	−694.8	−132.1
	±0.0029	±0.0002			
BFS-61-3	1.00040	0.9966	0.99302	−743.3	−170.4
	±0.0027	±0.0002			

the perturbed cross-sections library. Based on the core results, the data statistics as well as uncertainty calculation of the response quantities would be carried out.

The sensitivity analysis calculation is performed by either the direct perturbation method or the reverse sampling method. In the direct perturbation method, a two-way perturbation approach is applied and its sensitivity coefficient is calculated by the following formula:

$$S_j = \frac{\sigma_j \partial R}{\bar{R} \partial \sigma_j} \approx \frac{\sigma_j \mathrm{V} R}{\bar{R} \mathrm{V} \sigma_j} = \frac{\sigma_j (R_+ - R_-)}{\bar{R} \cdot 2\mathrm{V}\sigma_j} \tag{14}$$

where R_+ is the response value under positive perturbation conditions, R_- is the response value under negative perturbation conditions, and $\bar{R}$ is the response value under without perturbation.

The formula for calculating the sensitivity coefficient based on the reverse sampling method is:

$$S_\sigma^k = \left(A_{\sigma,\sigma}\right)^{-1} A_{k,\sigma} \tag{15}$$

where S_σ^k denotes the sensitivity coefficient of the response k to the cross-sections σ; $A_{\sigma,\sigma}$ is the relative covariance matrix of the cross-sections; $A_{k,\sigma}$ denotes the relative covariance matrix of the response k to the cross-sections.

3 Numerical results

To verify the cross-sections generation module, three kinds of fuel assemblies, including one-dimensional (1-D) flat fuel

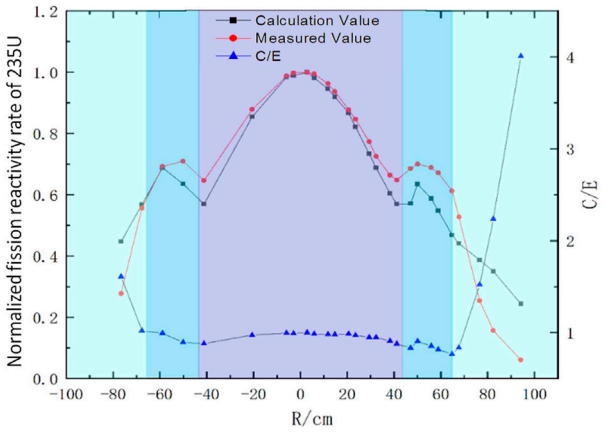

FIGURE 8
Results of normalized ^{235}U fission reactivity rate.

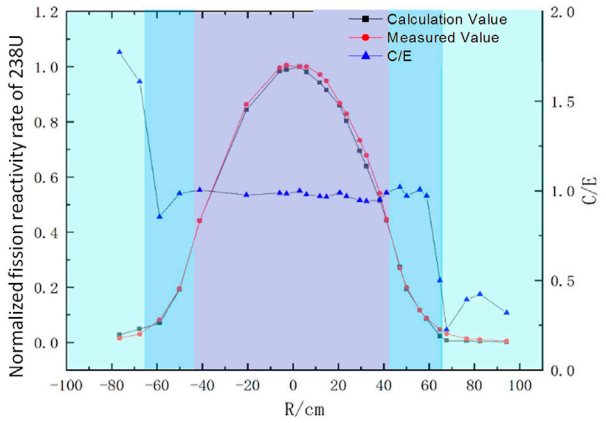

FIGURE 9
Results of normalized ^{238}U fission reactivity rate.

assembly of the critical experiment ZPPR-10B (Sanda et al., 2006a) as shown in Figure 3, 1-D cylindrical fuel assembly of MET-1000 benchmark (OECD/NEA, 2016), and 1-D cylindrical breeding assembly of the JOYO reactor (Yokoyama et al., 2006) are calculated. The accuracy and the ability to handle the heterogeneous effect can be verified. The reference solutions were obtained using the continuous energy Monte-Carlo code OpenMC. The results of eigenvalues are shown in Table 1, and the relative errors are within 200 pcm compared with the reference solutions.

Three lead-based critical experiments, including HEU-MET-FAST-027 (HMF27), PU-MET-FAST-035 (PMF35) and HEU-MET-FAST-057 (HMF57), are modeled for the further validation of MOCS. All three critical experiments consist of high enrichment fuel and lead reflector, the geometric and material parameters are shown in Table 2. The diagrams are shown in Figure 4.

The reference solutions were supported by the benchmark report which are measured values and results determined by the continuous energy Monte-Carlo code MCNP and KENO with different evaluation nuclear data files. The results of eigenvalues are shown in Table 3. Except for HMF57-1, the results of MOCS are in good agreement with the measured values. Compared with the Monte-Carlo code, the relative errors of eigenvalues are very small when the calculations were carried out with the same nuclear data file, and the maximum error is 100pcm.

The results of flux and reactivity rate are shown in Figure 5. Compared with the reference results, the flux at high energy has good calculation accuracy. The errors of flux below 0.01 MeV are much large. Due to the small proportion of the flux below 0.01MeV, they do not increase the error of the whole core calculation. The ratios between the results of MOCO and Monte-Carlo code show the same pattern. The results of fission reactivity rate and capture reactivity rate of different nuclides in the corresponding total reactivity rate agree well with the reference solution as shown in Table 4.

The Russian lead-cooled fast reactor BFS-61 (Manturov et al., 2006) has been modeled to validate MOSASAUR. The BFS-61 is a hexagonal core made of a stainless-steel tube with an outer diameter of 5.0 cm and a height of 216 cm arranged in accordance with a scheme of 5.1 cm rod spacing. Pie-shaped pellets are arranged in the stainless-steel tube in an axially laminated manner, and the pellet material includes fuel, coolant, and reflector and so on. The fuel rod is 86.64 cm high and made of 10 identical units. Each unit is shown in Figure 6. BFS-61 has three different core layouts as shown in Figure 7, and different types and numbers of rods are used.

The reference solution is provided by the benchmark report which contains the measured value and the calculation results of MCNP code. The results of MOSASAUR and MCNP are base on the same evaluation nuclear data files ENDF/B-VII.0. The summary of the eigenvalue results is shown in Table 5 and it is indicated that MOSASAUR has more than 500pcm difference compared with the measured value. While MOSASAUR agrees well with MCNP code based on the same nuclear data file.

The fission reactivity rates of different nuclides at several positions in the central plane were measured in the core BFS-61-1. The measured values are normalized based on that of the central plane of the core which is taken as the origin of R coordinate in Figure 8 and Figure 9. The degree of agreement between the calculation value and the measured value is expressed as the ratio C/E. The three different colored areas in the figures represent the active, reflective, and breeding zones. It can be found that the results of MOSASAUR have high accurate in active and reflective zones. The relative errors increase in the outer breeding zones. The flux value in this area is very small and the uncertainty is larger. In the modeling of the cross-section generation and core simulation, several details of the core structural components have been simplified.

4 Conclusion

The LBFR calculation code system named MOSASAUR developed by NPIC, CNNC is introduced in this paper. The deterministic two-step calculation strategy based on the homogenization theory is utilized in MOSASAUR. Four main functional modules and their models make up the whole code system. MOCS is used to generate the 33-group homogenized cross sections based on the ultrafine-group information (1968 groups). MOSN is used to correct the infinite flux spectrum of the single assembly with the reflective condition. MOCO is the simulation code for the whole life of LBFR. The sensitivity and uncertainty analysis module called SUN is used to evaluate and quantify the confidence of the calculated results. The preliminary verification and validation have been carried out, numerical results demonstrate that compared with the Monte-Carlo code, the relative errors of eigenvalues are smaller than 350pcm when the calculations were carried out with the same nuclear data file. Compared with the measured values, the errors will increase due to the simulation details and the measurement accuracy. The results indicated that MOSASAUR has good performances in dealing with lead-based cooled fast reactor. Modules of coupled neutron and gamma heating calculation, thermal-hydraulic feedback and core transient simulation are being developed and further verification and validation will be carried out later.

Data availability statement

The original contributions presented in the study are included in the article/supplementary material, further inquiries can be directed to the corresponding author.

Author contributions

BZ: Methodology, Software, Investigation, Numerical Analysis, Writing—Original Draft; LW: Methodology, Numerical Analysis; LL: Software, Investigation; CHZ: Numerical Analysis; XP: Methodology, Validation; MY: Methodology; BX: Methodology; CEZ: Numerical Analysis; LQ: Numerical Analysis; QW: Writing—Original Draft.

Funding

This research is supported by the National Natural Science Foundation of China (Approved number Nos. 12075228 and Nos. 12205283).

Acknowledgments

All the authors would like to thank NECP laboratory of Xi'an Jiaotong University for the architecture of the whole system and thank to North China Electric Power University for the help with the sensitivity and uncertainty analysis method.

Conflict of interest

The authors declare that the research was conducted in the absence of any commercial or financial relationships that could be construed as a potential conflict of interest.

Publisher's note

References

Archier, P., Palau, J. M., Vidal, J. F., Pascal, V., and Santandrea, S. (2016). New reference APOLLO3 calculation scheme for sodium cooled fast reactors: From sub-assembly to full-core calculations, Proceeding of the PHYSOR, May 1–5 2016, Sun Valley, USA.

Bouchard, J., and Bennett, R. (2008). Generation IV advanced nuclear energy systems. *Nucl. Plant J.* 26 (5), 42–45.

Cai, L. (2014). *Condensation et homogénéisation des sections efficaces pour les codes de transport déterministes par la méthode de Monte Carlo: Application aux réacteurs à neutrons rapides de GEN IV*. France: Doctoral Dissertation. Université Paris-Sud.

Derstine, K. L. (1984). *DIF3D: A code to solve one-, two-, and three-dimensional finite difference diffusion theory problems, ANL-82-64*. Lemont, Illinois: Argonne National Laboratory.

Downar, T., Kochunas, B., and Collins, B. (2016). *Validation and verification of the MPACT code*[C]. Sun valley ID United States: American Nuclear Society, 2961–2978.

Grimstone, N. M. Marseille, France. April 23–27, 1990. Accurate treatment of fast reactor fuel assembly heterogeneity with the ECCO cell code, Proceeding of PHYSOR90.

Hebert, A. *Applied reactor physics*[M]. Montreal, Canada: Presses Internationales Polytechnique, 2009.

Henryson, H., Toppel, B. J., and Sternberg, C. G. (1973). Paper Presented in Seminar on Nuclear Data Processing Codes. Ispra. Italy: ETOE-2/MC2-2/SDX, multigroup neutron cross section processing system

Heo, W., Kim, W., and Kim, Y., 2013. Feasibility of A Monte Carlo-deterministic hybrid method for fast reactor analysis. In: Proceeding of M&C 2013, May 5–9 2013, Sun Valley, Idaho.

Hu, D. P., and Yuan, H. Q. (1995). Reactor physics characteristics of lead cooled fast reactor-A new type fast nuetron reactor. *Nucl. Power Eng.* 16 (3), 195–198.

Lee, C. H., and Yang, W. S. (2012). *MC2-3: Multigroup cross section generation code for fast reactor analysis, ANL/NE-11-41*. Lemont, Illinois: Argonne National Laboratory.

Li Z, M., Igor Li, M., and Igor, Z. Jeju Korea. April 16–20, 2017. A new tone's method in APOLLO3 and its application to ZPPR benchmarks, Proceeding of the M&C2017.

Liu, S. H., Wang, Z. J., Jia, H., He, Y., Dou, W. P., Qin, Y. S., et al. (2017). Physics design of the CIADS 25MeV DEMO facility. *Nucl. Instrum. Methods Phys. Res. Sect. A Accel. Spectrom. Detect. Assoc. Equip.* 843, 11–17. doi:10.1016/j.nima.2016.10.055

Macfarlane, R. E., and Muir, D. W. (1994). *The NJOY nuclear data processing system*. Los: Alamos National Laboratory.

Manturov, G., Kochetkov, A., Sememnov, M., et al. (2006). *BFS-62-3Aexperiment: Fast reactor core with U and U-Pu fuel of 17% enrichment and partial stainless steel reflector*. Paris, France: NEA/NSC.DOE, 1. IRPHE Handbook.

Nikitin, E., Fridman, E., Mikityuk, K., et al. (2015). Solution of the OECD/NEAneutronic SFR benchmark with serpent-dyn3d and serpent-PARCS code systems. *Ann. Nucl. Energy* 75, 492497. doi:10.1016/j.anucene.2014.08.054

OECD/NEA (2016). *Benchmark for neutronic analysis of sodium-cooled fast reactor cores with various fuel types and core sizes NEA/NSC/R*. Paris, France: OECD/NEA 9.

Palmiotti, G., Lewis, E. E., and Carrico, C. B. (1995). *Variant: VARIational anisotropic nodal transport for multidimensional cartesian and hexagonal Geometry calculation, ANL-95/40*. Lemont, Illinois, Argonne National Laboratory.

Rachamin, R., and Kliem, S. (2017). Validation of the dyn3d-serpent code system for SFR cores using selected BFS experiments. Part I: Serpent calculations. *Ann. Nucl. Energy* 102, 158–167. doi:10.1016/j.anucene.2016.12.023

Sanda, T., Ishikawa, M., Lell, R. M., et al. (2006a). *ZPPR-10Bexperiment: A 650 MWe-class sodium-cooled MOX-fueled fbr homogeneous core mock-up critical experiment with two enrichment zones, seven control rods and twelve control rod positions ZPPR-LMFR-EXP-005*. Paris, France: NEA/NSC/Doc. OECD/NEA 1.

Shemon, E. R., Smith, M. A., and Lee, C. H. (2017). Jeju, Korea. April 16–20, 2017.Direct neutronics modeling approach for deformed core analysis using PROTEUS, Proceeding of M&C 2017.

Wang, K., Li, Z. G., She, D., Liang, J., Xu, Q., Qiu, Y., et al. (2015). Rmc – a Monte Carlo code for reactor core analysis. *Ann. Nucl. Energy* 82, 121–129. doi:10.1016/j.anucene.2014.08.048

Wu, Y. C. (2016). Design and R&D progress of China lead-based reactor for ads research facility. *Engineering* 2 (1), 124–131. doi:10.1016/j.eng.2016.01.023

Xu, M. (2009). Fast reactor and sustainable nuclear energy development in China. *China Nucl. Power* 2 (2), 106–120.

Yokoyama, K., Shono, A., Sanda, T., et al. (2006). *Japans experimental fast reactor JOYOMKI core: Sodium-cooled uranium-plutonium mixed oxide fueled fast core surrounded by UO2 blanket JOYO-LMFR-RSR-001*. Paris, France: NEA/NSC/Doc.OECD/NEA 1.

Zhang, B., Li, Y. Z., Wu, H. C., Cao, L., and Shen, W. (2016). Evaluation of pin-cell homogenization techniques for PWR pin-by-pin calculation. *Nucl. Sci. Eng.* 186 (2), 134–146. doi:10.1080/00295639.2016.1273018

Zheng, Y. Q., Du, X. N., Xu, Z. T., Zhou, S., Liu, Y., Wan, C., et al. (2018). Sarax: A new code for fast reactor analysis part I: Methods. *Nucl. Eng. Des.* 340, 421–430. doi:10.1016/j.nucengdes.2018.10.008

Zheng, Y. Q., Qiao, L., Zhai, Z. A., Du, X., and Xu, Z. (2018). Sarax: A new code for fast reactor analysis part II: Verification, validation and uncertainty quantification. *Nucl. Eng. Des.* 331, 41–53. doi:10.1016/j.nucengdes.2018.02.033